Porphyrinic metal-organic framework nanorod-based dual-modal nanoprobe for sensitive phosphate detection

Changming Cheng[a,c], Ruolin Zhang[a], Jiuhai Wang[a], Yu Zhang[d], Ying Huang[b], Mo Yang[a*]*

[a]*Department of Biomedical Engineering, The Hong Kong Polytechnic University, Hung Hom, Kowloon, Hong Kong SAR, PR China*

[b]*State Key Laboratory of Environment-friendly Energy Materials & School of Materials Mcience and Engineering, Southwest University of Science and Technology, Mianyang 621010, PR China*

[c]*Institute of Nuclear Physics and Chemistry, China Academy of Engineering Physics (CAEP), Mianyang 612900, PR China*

[d]*Mechanical and Automotive Engineering, Royal Melbourne Institute of Technology, Melbourne, Australia*

Corresponding authors

E-mail address: Mo.Yang@polyu.edu.hk (Mo Yang); huangy@swust.edu.cn (Ying Huang)

The following publication Cheng, C., Zhang, R., Wang, J., Zhang, Y., Xiong, S., Huang, Y., & Yang, M. (2020). Porphyrinic metal–organic framework nanorod-based dual-modal nanoprobe for sensing and bioimaging of phosphate. ACS applied materials & interfaces, 12(23), 26391-26398 is available at https://doi.org/10.1021/acsami.0c06057

TOC

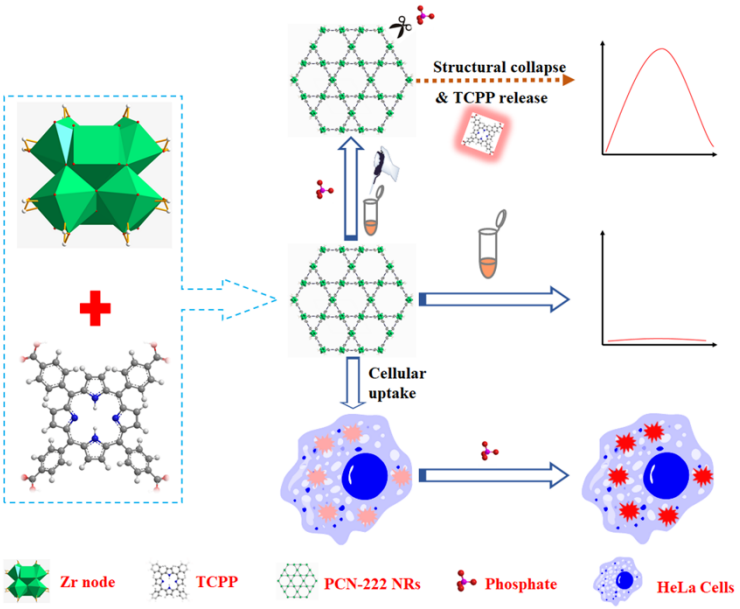
Structural collapse
& TCPP release
Cellular
uptake
Zr node
TCPP
PCN-222 NRs
Phosphate
HeLa Cells

Abstract

In the past few years, metal-organic frameworks (MOFs) have attracted great attention due to their unique chemical/physical properties and great potential in various applications. Herein, a typical porphyrinic based MOFs (i.e., PCN-222) with nanorod shape and good water dispersibility were constructed by coordination of zirconium node with tetrakis(4-carboxyphenyl)porphyrin (TCPP) ligand. Phosphate is a typical anion in the natural environment and biology species. Due to the high affinity of the zirconium node in PCN-222 nanorods (PCN-222 NRs) for phosphate, the structural collapse of PCN-222 NRs may be triggered in the presence of phosphate, resulting in the release of TCPP ligand from the PCN-222 NR framework as well as the enhancement of fluorescence emission and UV-vis absorbance. Accordingly, the first demonstration of dual-modal (fluorescent and colorimetric) "Signal-On" nanoprobe based on PCN-222 NRs was established for the sensitive and selective determination of phosphate over a wide concentration range with a detection limit down to 23 nM where zirconium node and TCPP ligand served as recognition motif and indicator for phosphate detection, respectively. The practical application of PCN-222 NR-based nanoprobe for phosphate detection in the real samples was successfully evaluated. Moreover, benefiting from the good biocompatibility and water dispersibility of PCN-222 NRs, the proposed nanoprobe was successfully employed in the intracellular imaging of phosphate, revealing its promising applications in the biological science. The present work would greatly extend the potential of nanostructured MOFs in the sensing and biological applications.

Keywords

Metal-organic framework (MOF); nanorods; signal on; dual-modal nanoprobe, intracellular imaging; phosphate

Introduction

Recently, metal-organic frameworks (MOFs), also named as porous coordination networks or coordination polymers, have received a lot of attention due to their charming properties (e.g. porosity, structural diversity and tenability), which have potential applications in diverse fields including gas storage/separation,[1,2] catalysis,[3,4] drug delivery/therapy,[5,6] sesning,[7,8] et al. However, it should be noted that the research of MOFs in the sensing field is still in its infancy and should be in-depth explored in the future work. Furthermore, it was reported nanostructured MOFs (NMOFs) with different morphologies such as zero-dimensional nanoparticles/nanocrystals, one-dimensional nanoneedles/nanorods and two-dimensional nanosheets/nanoplates would exhibit better analytical performance in comparison to their bulk-phase counterparts due to high surface areas, abundant accessible active sites and unique size-dependent properties of NMOFs. In the previous work, some types of chemical sensors and biosensors (i.e., fluorescent, colorimetric, electrochemical, electrochemiluminescent and photoelectrochemical sensors) based on NMOFs have been developed for the sensitive and selective determination of various analytes including metal ions, anions and bio-related molecules.[9-13] Recently, our group reported for the first time the preparation of ultrasmall Zn-MOF-74 nanodots and their application in the colorimetric sensing of Fe^{3+} due to the highly selective interaction between the organic ligand in Zn-MOF-74 nanodots and Fe^{3+} . .

Among diverse functional NMOFs used in chemical sensing and biosensing fields, one of the most promising candidates should be luminescent NMOFs, which could be employed as effective nanoprobes for the exploitation of novel fluorescent and electrochemiluminescent sensors with high sensitivity and selectivity. Since chemical sensing and biosensing processes are mainly performed in the aqueous medium, the

stability of NMOFs in the water should be a particularly important issue in the sensing field, especially in the biosensing field. As such, water-stable and fluorescent zirconium porphyrinic NMOFs (e.g. MOF-525,[15] PCN-222/MOF-545,[13,16] and PCN-224[17-20]) prepared by using zirconium as the metal node and tetrakis(4-carboxyphenyl)porphyrin (TCPP) as the organic ligand, would have great potential in the development of novel chemical sensors and biosensors due to its high stability. However, to the best of our knowledge, the current biological applications of fluorescent zirconium porphyrinic NMOFs were mainly used in bioimaging and therapy,[16-19] while there are few reports on the biosensing applications performed in the aqueous medium.[13,20] In addition, it is noteworthy that previous biological applications of zirconium porphyrinic NMOFs mainly focused on using the unique property of individual structural component (zirconium node or TCPP ligand).. TCPP ligand could emit intense fluorescence,[15] generate singlet oxygen[16] and exhibit catalytic activity,[21] while zirconium node could act as the binding site for molecules.[13,22] The major contribution of the present work is to expand the potential application of zirconium porphyrinic NMOFs in the sensing field by taking both advantages of zirconium node and TCPP ligand assembled in the framework of porphyrinic NMOFs.

As one of anionic species, phosphate has attracted considerable attention in wide fields such as environment and biology. In natural environment, phosphate was one of typical pollutants and its concentration in the water sample was of great concern.[23] What's more, phosphate was the hydrolysis product of diverse alkaline phosphatase substrates, which was one of the most important indicators in health.[24,25] To date, numerous analytical techniques including fluorescence, electrochemistry, electrochemiluminescence and chromatography have been employed for phosphate

determination. Compared with other sensing strategies, fluorescence would be of particular interest owing to its inherent virtues of high sensitivity, good reproducibility, simple operation, less consumption, and portability. As is well-known, not only can fluorescent sensors be used for the phosphate detection in vitro, but also would they exhibit great potential in the real-time detection as well as intracellular monitoring of phosphate in the living cells, inspiring the development of high-efficiency fluorescent probes towards phosphate. However, it should be noted that some fluorescent probes in previous reports generally worked in the organic solvent or organic solvent/water mixture solution,[26-30] due to their poor solubility/dispersibility in the aqueous medium, hindering their further practical applications. Recently, several fluorescent sensing platforms have been proposed for phosphate detection in the aqueous medium. For instance, Zhao et al.[23] developed a europium-adjusted carbon dot-based off-on fluorescence sensor for phosphate detection due to the competitive coordination between phosphate and carboxylate groups on carbon dots towards europium; Chu et al.[31] fabricated a europium MOF film-based luminescence "Signal-Off" sensor for the determination of phosphate due to the ligand displacement approach; Dai et al.[32] developed a silver nanoclusters/Zn^{2+}-Imidazole-2-carboxaldehyde (Zn-ICA) shell composite-based fluorescence sensor for the ratiometric determination of phosphate due to the high affinity between phosphate and Zn^{2+}; Yang et al.[33] and Zhang et al.[34] established UiO-66-NH_2 and UiO-TCPP MOF-based fluorescence strategies for "Signal-On" sensing of phosphate due to the high affinity of phosphate towards the zirconium node in UiO-type MOFs. However, it is also of great importance to exploit novel fluorescence nanoprobes for phosphate detection in the aqueous medium as well as intracellular imaging of phosphate in the living cells. As far as we know, there is few

nanoprobe based on porphyrinic NMOFs for the sensing and intracellular imaging of phosphate until now.

In the present work, zirconium was employed as the metal node and TCPP was employed as the organic ligand for the preparation of a typical kind of zirconium porphyrinic MOFs nanorods (PCN-222 NRs) with good water stability and dispersibility. Due to the high affinity between zirconium node in PCN-222 NRs and phosphate, the structure collapse of PCN-222 NRs would happen after exposure to phosphate, and distinct fluorescence emission and UV-vis absorbance enhancement could be observed. Thus, a type of dual-modal (fluorescent and colorimetric) "Signal-On" probe based on PCN-222 NRs was firstly proposed for the determination of phosphate. It's expected that the proposed dual-modal nanoprobe would improve the reliability and precision of the analysis results. It's observed in the PCN-222 NR-based nanoprobe that the fluorescent detection mode displayed a linear response towards phosphate in the concentration range of 0.25-100 μM with a detection limit of 0.023 μM, whereas colorimetric detection mode displayed a linear response towards phosphate in the concentration range of 0.25-25 μM with a detection limit of 0.22 μM. The practical application of the PCN-222 NR-based dual-modal nanoprobe in real water samples was evaluated with acceptable results. Furthermore, the potential application of PCN-222 NRs in the intracellular imaging of phosphate was studied by using HeLa cells as the cells model. To the best of our knowledge, this is the first report on the construction of PCN-222 NR-based nanoprobe towards phosphate in the water sample and living cells. It is anticipated that NMOFs would have great potential in analytical chemistry and biology.

Experimental Section

Chemicals and reagents

Zirconium chloride ($ZrCl_4$, 99.95 %), benzoic acid (BA, 99.5 %) and *N*,*N*-dimethylformamide (DMF, 99.9 %) were purchased from J&K Scientific Ltd. Cetyltrimethyl ammonium bromide (CTAB, 99 %), 4-(2-hydroxyethyl)-1-piperazineethanesulfonic acid (HEPES) buffer solution and 3-(4,5-dimethylthiazol-2-yl)-2,5-diphenyltetrazolium bromide (MTT) were purchased from Sigma-Aldrich. Polyethylene glycol (PEG, Mw=6000) was purchased from TCI (Shanghai) development Co., Ltd. Tetrakis(4-carboxyphenyl)porphyrin (TCPP, 97 %) was purchased from Frontier Scientific. Other chemicals of analytical grade were used as received without further purification. Ultrapure water (18.2 MΩ·cm) was used throughout the work.

Characterization

UV-vis absorbance and fluorescence spectra were measured on the Ultrospec 2100 Pro spectrophotometer and Edinburgh FLS920 photoluminescence spectrometer, respectively. Powder X-ray diffraction (XRD) patterns were recorded on the Rigaku SmartLab diffractometer by using Cu Kα radiation. Transmission electron microscope (TEM) and scanning electron microscope (SEM) images were captured on the JEOL Model JEM-2100F electron microscope and JEOL Model JSM-6700F field emission electron microscope, respectively. Zeta potential measurement was performed on the Malvern ZEN 3600 Zetasizer Nano System. MTT assay was conducted on the Tecan Infinite 200 microplate reader. Confocal fluorescence images were recorded on the Olympus FV1000-IX81 confocal laser scanning biological microscope and a Leica TCS-SP5 confocal system.

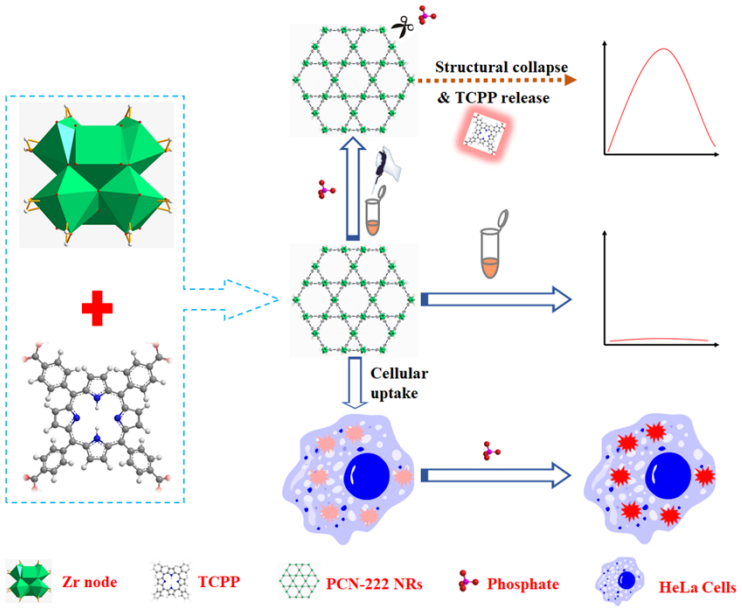

Scheme 1. Schematic representation of PCN-222 NR as nanoprobe for sensing and intracellular imaging of phosphate.

Preparation of PCN-222 NRs

PCN-222 NRs were prepared by the previously reported solvothermal protocol with slight modification,[16] as shown in Scheme 1. Typically, $ZrCl_4$ (20 mg), BA (200 mg), CTAB (66.7 mg), PEG (66.7 mg) and TCPP (6.67 mg) were dissolved in DMF (6.67 mL) under sonication for ca. 10 min. Then the resulting mixture was transferred into Teflon-lined autoclave (20 mL) and heated at 120 ℃ in the oven for 12 h. After cooling down naturally to room temperature, the product was obtained via centrifugation at 13500 rpm, followed by washing with DMF, ethanol and water for several times. Finally, the product in dry powder was obtained by freeze-drying overnight and kept in darkness for further use.

Fluorescent/colorimetric sensing of phosphate

Both fluorescent and colorimetric detections of phosphate were carried out in the 20 mM HEPES buffer solution. Firstly, the mixture solution containing 50 mg L^{-1} of PCN-222 NRs and a certain concentration (0.0-200 μM) of phosphate were incubated for 4 h at room temperature. Secondly, the mixture solution was centrifuged at 13500 rpm and the resulting supernatant was collected for the corresponding fluorescence and UV-vis absorbance spectra measurements. In order to testify the effects of buffer pH (5.5-8.0) and potential interfering species (i.e., Cl^-, SO_4^{2-}, NO_3^-, NO_2^-, Ac^-, CO_3^{2-}, GSH, Ca^{2+}, K^+, Na^+, Mg^{2+}) on fluorescent and colorimetric response of the PCN-222 NR-based nanoprobe, similar procedures

were carried out except the concentrations of phosphate (or interfering species) were fixed to 100 μM and 25 μM for fluorescent and colorimetric detection mode, respectively.

Intracellular imaging of phosphate

MTT assay was conducted to evaluate the cytotoxicity of PCN-222 NRs to HeLa cells. Firstly, HeLa cells were seeded in a 96-well plate at a density of 1.0×10^4 well^{-1} and cultured in Dulbecco's modified Eagle medium in the presence of 10 % fetal bovine serum and 1 % penicillin/streptomycin in an incubator (37 °C, 5 % CO_2) for 24 h. Then, PCN-222 NRs with different concentrations (10~50 mg L^{-1}) were added into the well (100 μL well^{-1}) and cultured for 24 h. After discarding the solution, 100 μL cell medium containing MTT (10 μL, 5 g L^{-1}) was added into each well, and further incubated for 4 h. Then, 100 μL dimethyl sulfoxide was added into each well to replace the cell medium, and another 10 min incubation was performed. The control group was treated in the same procedure in the absence of PCN-222 NRs. Finally, absorbance value at the wavelength of 490 nm in each well was recorded and the cell viability was calculated with the formula (1):

$$\text{Cell viability (\%)}=\frac{A_s-A_b}{A_c-A_b}\times100\ \% \quad (1)$$

where A_s, A_b, A_c were absorbance values of experimental group, blank well and control group, respectively.

Prior to intracellular phosphate imaging, HeLa cells were cultured in dishes at a density of 1.0×10^6 well^{-1}, treated with 25 mg L^{-1} PCN-222 NRs for 8 h (37 °C, 5 % CO_2), and washed with Dulbecco's modified Eagle medium for three times. Then, exogenous phosphate with a final concentration of 100 μM was added into dishes, and HeLa cells were incubated for another 8 h. In addition, the control experiment was performed in the similar procedure in the absence of PCN-222 NRs and phosphate. After washing with Dulbecco's modified Eagle medium for three times, confocal fluorescence images of HeLa cells were captured at 550~800 nm range upon excitation at 405 nm.

Results and discussion

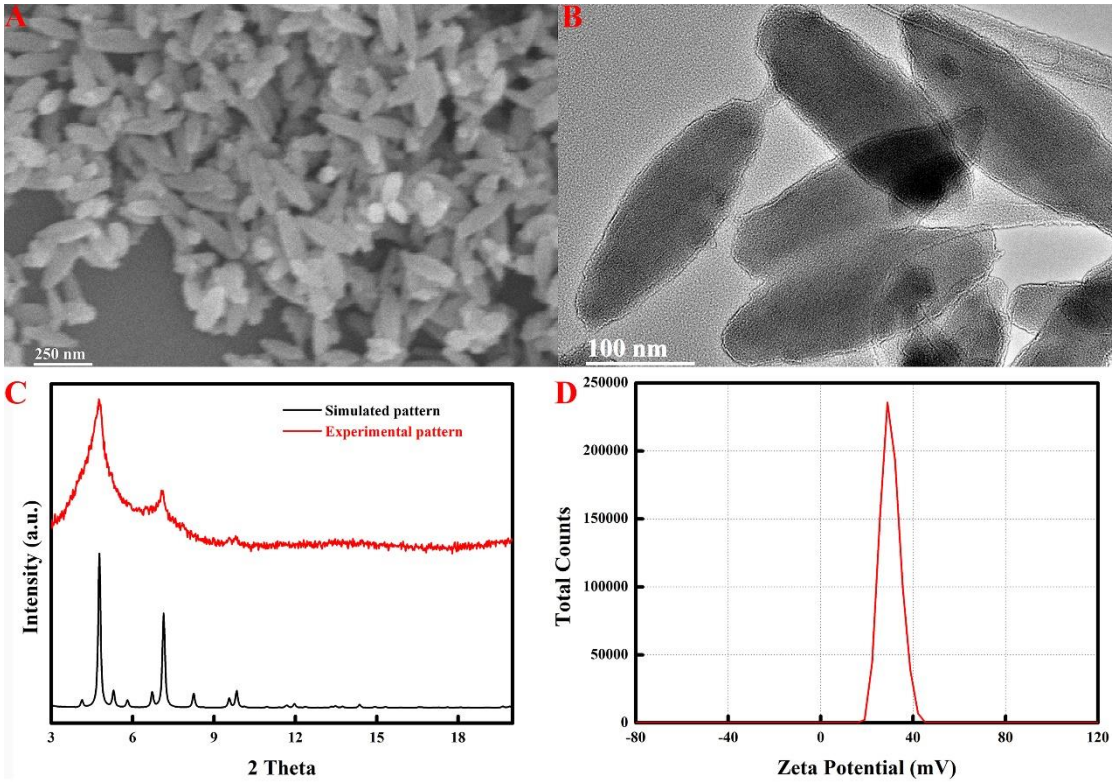

Figure 1. (A) SEM image, (B) TEM image, (C) XRD pattern, and (D) Zeta-potential of the as-prepared PCN-222 NRs.

Firstly, the morphology of the as-prepared sample was investigated with SEM and TEM images, as depicted in Figure 1 A and 1B. It can be clearly observed that the sample possessed the typical nanorod shape with lateral dimensions of ca. 80 nm × 200 nm (diameter × length). Then, the crystalline structure of the sample was identified with XRD measurement. Figure 1C displayed the XRD pattern of the sample, matching well with the simulated XRD pattern of PCN-222, although diffraction peaks of the sample were much broader compared to the simulated ones, possibly attributing to its nanostructure. The similar results have been widely reported in the previous work.[16,35] Figure 1D displayed the zeta potential of the sample in the water. The sample was positively charged with a surface zeta potential of ca. 30.2 mV, indicating that it may be dispersed well in the water medium. Based on aforementioned results, we can get a conclusion that the sample composed of PCN-222 NRs was successfully synthesized in the present work by solvothermal reaction of $ZrCl_4$ and TCPP. The similar synthesis route was reported in the previous work[16] while the reaction time was reduced to 12 h in our work.

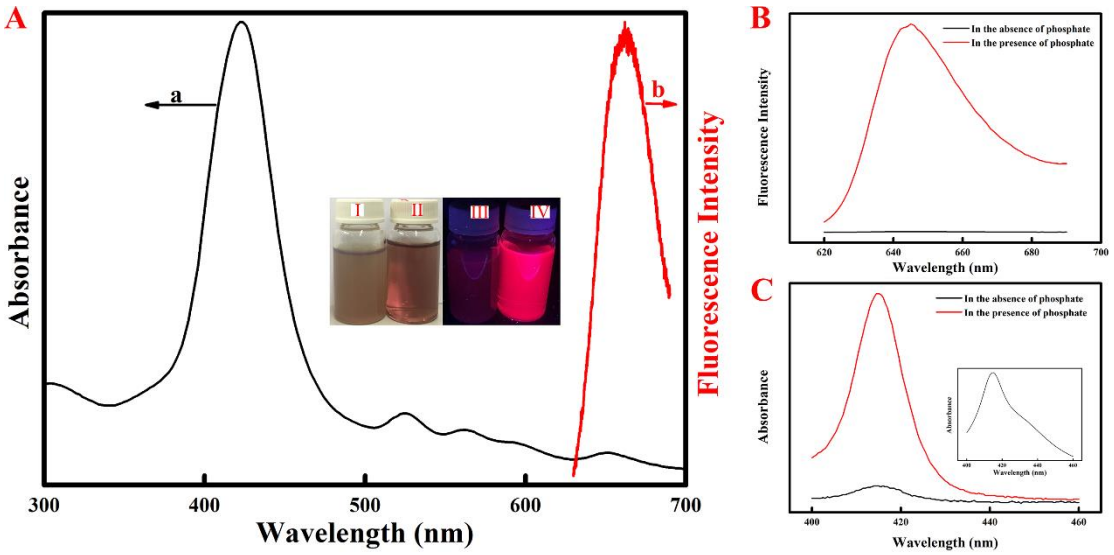

Figure 2. (A) Spectroscopic characterization of PCN-222 NRs, (a) UV-vis absorbance and (b) fluorescence emission spectra of PCN-222 NRs aqueous dispersion, Inset in Figure 2A: photographs of PCN-222 NRs in the water under the (I, II) ambient and (III, IV) UV light irradiation in the (I, III) absence and (II, IV) presence of phosphate. (B) Fluorescence emission and (C) UV-vis absorbance spectra of the supernatant obtained by incubating of PCN-222 NRs with and without phosphate in HEPES buffer solution for 4 h and centrifuging. Inset in Figure 2C: the UV-vis absorbance spectrum of PCN-222 NRs dispersion in HEPES buffer solution (20 mM, pH 7.0).

Then, spectroscopic (i.e., fluorescence, UV-vis absorbance) behaviors of the as-prepared PCN-222 NRs in the water were studied, as depicted in Figure 2A. The maximum absorbance peak located at 424 nm as well as four shoulder peaks in the range of 500-700 nm could be clearly observed on the UV-vis absorbance spectrum (curve *a* in Figure 2A), while a maximum fluorescence emission peak centered at 662 nm could be recorded upon excitation at 464 nm (curve *b* in Figure 2A). The similar phenomenon has been reported in the previous work.[16] From the inset of Figure 2A, we can see that PCN-222 NRs could be dispersed well in the water, and a weak red fluorescence could be obtained under the UV light irradiation, consistent with the results of zeta potential and fluorescence spectrum measurements (Figure 1D and 2A). Furthermore, it's found that the weak fluorescence of PCN-222 NRs could be enhanced significantly after introducing phosphate into PCN-222 NRs water dispersion. As displayed in the Inset of Figure 2A, "Signal-On" bright red fluorescence could be observed by the naked eye in the presence of phosphate under UV light irradiation. Inspired by the good water dispersibility of PCN-222 NRs and their response towards phosphate, it was anticipated that the as-prepared PCN-222 NRs could be served as the high-efficiency candidate for chemical sensor/biosensor towards phosphate. Then, in order to

further explore the influence of phosphate on spectroscopic behaviors of PCN-222 NRs as well as the potential application of PCN-222 NRs in the sensing field, the mixture of PCN-222 NRs and phosphate was incubated in HEPES buffer solution for 4 h and the resulting supernatant after centrifuge was used to fluorescence emission and UV-vis absorbance measurements. Figure 2B displayed the fluorescence emission spectra of the resulting supernatant in the absence and presence of phosphate in the HEPES buffer solution (20 mM, pH=6.5), respectively. The supernatant obtained in the absence of phosphate showed negligible weak fluorescence emission signal (black curve in Figure 2B), whereas strong fluorescence emission centered at 646 nm was recorded on the supernatant obtained in the presence of phosphate (red curve in Figure 2B), confirming the enhancement of phosphate on the fluorescence emission signal and consistent with phenomenon shown in the Inset of Figure 2A. Figure 2C displayed the UV-vis absorbance spectra of the resulting supernatant in the absence and presence of phosphate in the HEPES buffer solution (20 mM, pH=7.0), respectively. The enhancement on the UV-vis absorbance signal could also be observed upon addition of phosphate. A weak absorbance peak could be observed on the supernatant even in the absence of phosphate (black curve, Figure 2C), which could be attributed the PCN-222 NRs residue in the supernatant due to the good dispersibility of PCN-222 NRs in the HEPES buffer solution. It could be validated by the similar UV-vis absorbance spectrum of PCN-222 NRs in the HEPES buffer solution, as depicted in the Inset of Figure 2C. Furthermore, it should be noted that both fluorescence emission and UV-vis absorbance spectra of the resulting supernatant obtained in the presence of phosphate in the HEPES buffer solution exhibited blue shift compared with fluorescence emission and UV-vis absorbance spectra of PCN-222 NRs in the water. The possible reason would be discussed in detail in the following working mechanism section (vide infra). In consideration of aforementioned results, it could be expected that a dual modal “Signal-On” sensing strategy based on PCN-222 NRs would be proposed for the determination of phosphate, due to the unique response of PCN-222 NRs towards phosphate.

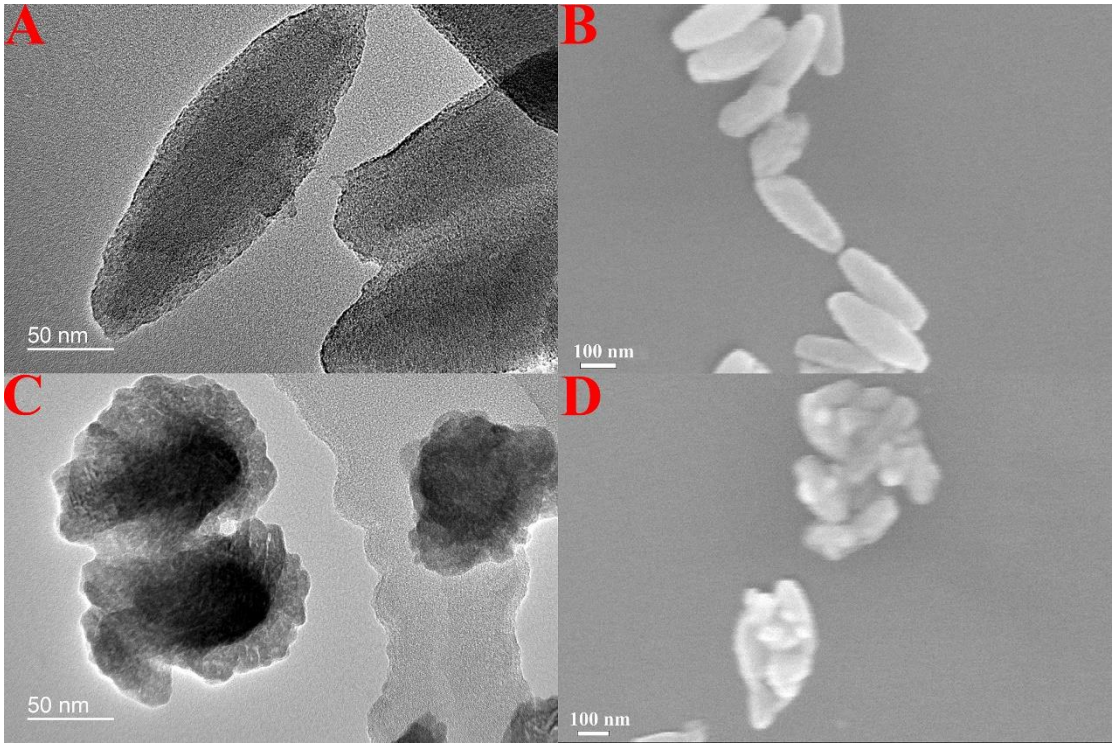

Figure 3. (A, C) TEM and (B, D) SEM images of PCN-222 NRs (A, B) before and (C, D) after incubation with phosphate.

The plausible working mechanism of phosphate-triggered fluorescence emission and UV-vis absorbance enhancement was studied. Chen et al.[36] reported that zirconium MOF (NU-1000) would degrade to release the encapsulated guest molecule (insulin) as well as linker in the presence of phosphate since phosphate would irreversibly cleave the node-linker bonds. Yang et al.[33] reported that phosphate exhibited high affinity towards the zirconium node and demonstrated a competitive coordination effect with the carboxylic group of organic ligand in the zirconium MOF (UiO-66-NH_2), which would weaken the interaction between zirconium node and organic ligand. Accordingly, we speculated that the structure of PCN-222 NRs would collapse after exposure to phosphate, since phosphate could combine zirconium node to form more stable zirconium-phosphate bond and deprive irreversibly zirconium-carboxylate bond in the host framework of PCN-222 NRs due to the stronger binding between zirconium node and phosphate compared with that between zirconium node and carboxyl group of TCPP, thereby initiating the release of free TCPP ligand as well as enhancement of fluorescence emission and UV-vis absorbance signals. As demonstrated by previous work,[37] the inherent fluorescence of TCPP has been employed for the development of a signal amplification method for biomolecule detection. In the present work, PCN-222 NRs can be removed by centrifuge in the absence of phosphate, and the resulting supernatant

exhibited weak fluorescence emission and UV-vis absorbance signals. On the other hand, in the presence of phosphate, the free TCPP released from the host framework of PCN-222 NRs during the structure collapse can not be removed by centrifuge and would stay in the supernatant, leading to the increase of fluorescence emission and UV-vis absorbance signals.

As such, TEM, SEM, and XRD measurements were performed to monitor the possible structural change of PCN-222 NRs induced by phosphate, demonstrating the hypothesis proposed in this work. Figure 3 displayed TEM and SEM images of PCN-222 NRs before and after incubation with phosphate. The morphology damage of pristine PCN-222 NRs could be observed clearly in the presence of phosphate. The original morphology of PCN-222 NRs was typical nanorod, as depicted in Figure 1A, 1B, 3A and 3B; however, after exposure to phosphate, it would change into irregular nanoparticle structure, as depicted in Figure 3C and 3D, implying the structure collapse of PCN-222 NRs triggered by phosphate due to the highly specific coordination between zirconium node in the host framework of PCN-222 NRs and phosphate.

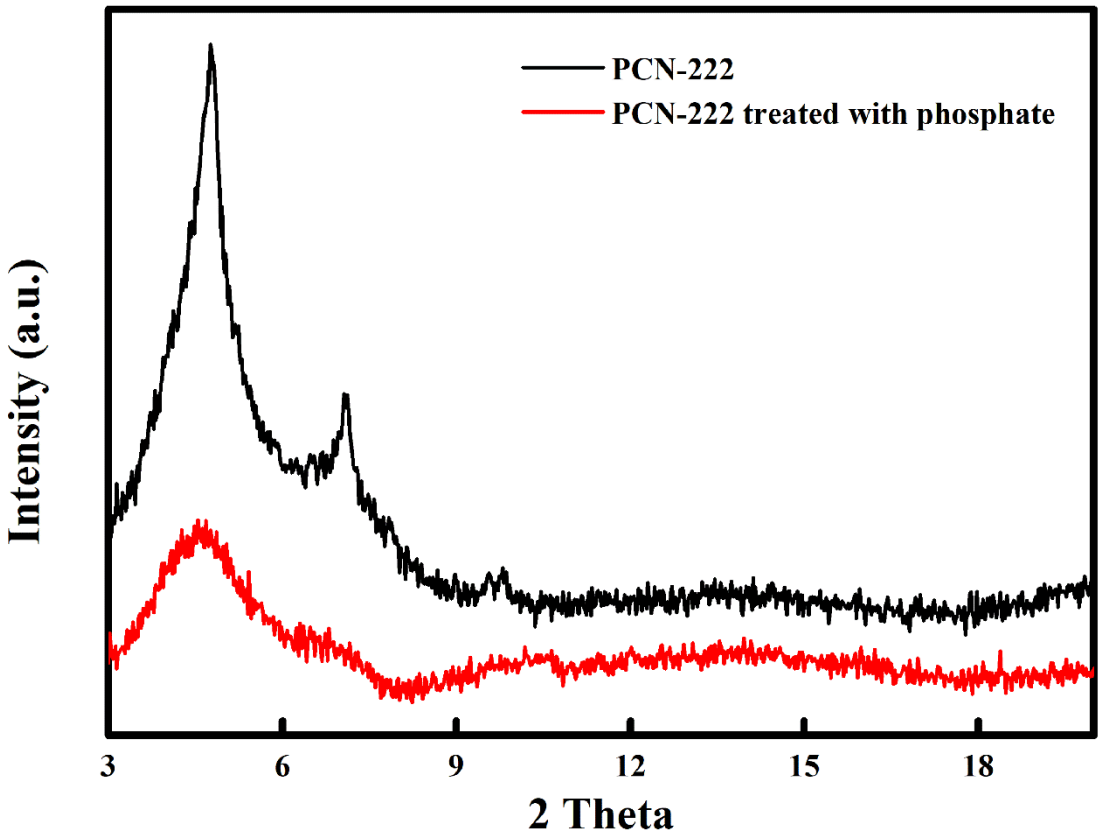

Figure 4. XRD patterns of PCN-222 NRs before and after treatment with phosphate.

In order to further verify the possible structure collapse hypothesis of PCN-222 NRs in the presence of phosphate, apart from TEM and SEM measurements, the XRD pattern of PCN-222 NRs after incubation with phosphate was recorded (red curve in Figure 4), which was obviously different from the XRD pattern of pristine PCN-222 NRs (black curve in Figure 4). For instance, after incubation of PCN-222 NRs with phosphate, characteristic diffraction peaks of PCN-222 NRs disappeared and/or weakened, indicating the damage of crystal structure. The similar phenomena were reported in the previous works where the crystal structures of MOF-5[38] or lanthanide coordination supramolecular networks (CSN-Eu)[31] could be damaged by phosphate due to the strong coordination of metal ions (i.e., Zn^{2+}, Eu^{3+}) with phosphate. Therefore, we may get a conclusion that the presence of phosphate would induce the structure collapse of PCN-222 NRs, resulting in the release of free TCPP ligand from the host framework of PCN-222 NRs. Furthermore, the fluorescence emission and UV-vis absorbance spectra with the maximum peaks at 646 nm and 414 nm obtained on the supernatant were similar to those of free TCPP.[16,37] The enhanced fluorescence emission and UV-vis absorbance signals in the supernatant may come from the

released free TCPP away from the framework of PCN-222 NRs rather than PCN-222 NRs themselves, based on which, the blue-shift on the fluorescence emission and UV-vis absorbance spectra (Figure 2B, 2C) was reasonable. The plausible working mechanism for the enhancement of phosphate on the fluorescence emission and UV-vis absorbance signals was illustrated in Scheme 1.

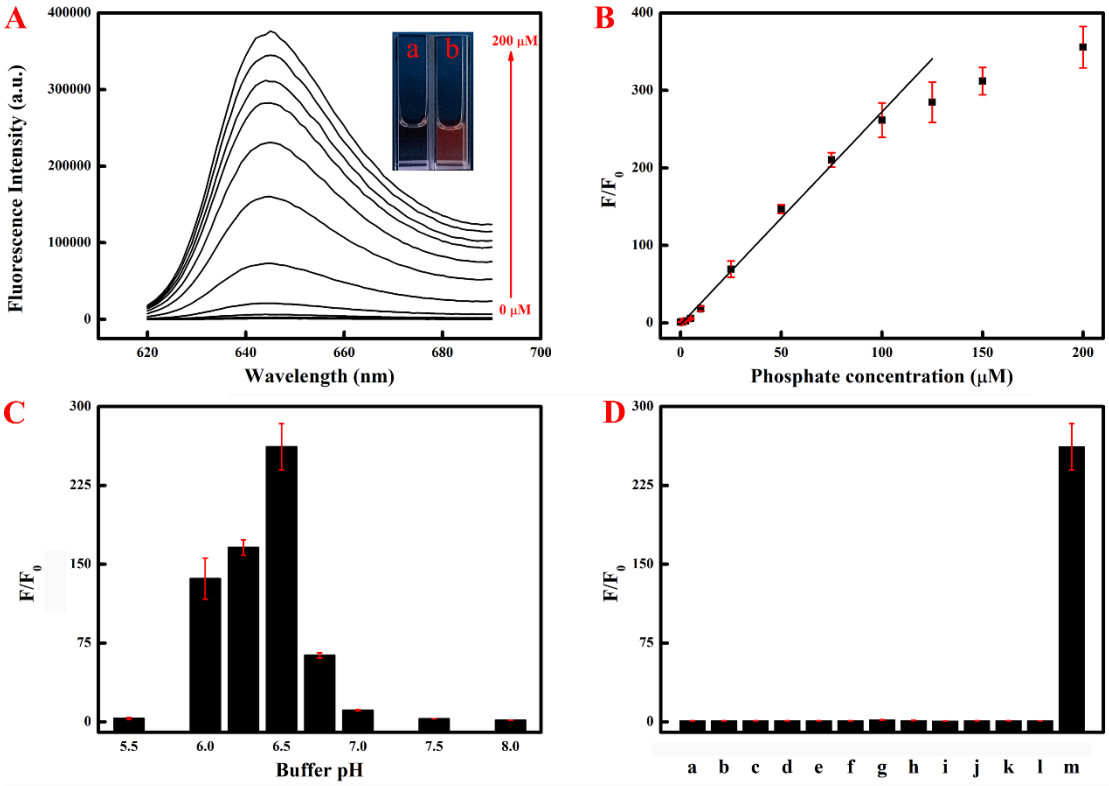

Figure 5. Fluorescent detection mode for phosphate. (A) Fluorescence spectra of supernatant obtained by incubating PCN-222 NRs with phosphate at different concentrations (0-200 μM) in the HEPES buffer solution (20 mM, pH 6.5) and centrifuging, (B) Plot of fluorescence emission enhancement (F/F_0) against phosphate concentration, (C) The effect of buffer pH on the fluorescence enhancement, (D) Selectivity experiments, a) blank, b) Cl^-, c) SO_4^{2-}, d) NO_3^-, e) NO_2^-, f) Ac^-, g) CO_3^{2-}, h) GSH, i) Ca^{2+}, j) K^+, k) Na^+, l) Mg^{2+}, m) phosphate with the concentration of 100 μM, where F_0 and F represented fluorescence emission intensities of the nanoprobe before and after exposure to the respective analyte, respectively. Inset in Figure 5A: photographs of supernatant obtained in the (a) absence and (b) presence of phosphate under UV light irradiation.

Based on abovementioned results, we speculated that a dual-modal (i.e., fluorescent and colorimetric) nanoprobe on the basis of PCN-222 NRs composed of zirconium node and TCPP ligand could be proposed for the detection of phosphate by using zirconium node and TCPP ligand as recognition site and reporter, respectively. Firstly, for the fluorescent detection mode, the effect of phosphate concentration on the fluorescence emission signal was investigated. Figure 5A displayed the fluorescence spectra of the supernatant, which was obtained by incubating PCN-222 NRs with phosphate at different concentrations and subsequently centrifuging. It can be clearly observed that the fluorescence emission intensity increased proportionally with the concentration of phosphate in the range from 0 μM to 200 μM. As depicted in the Inset of Figure 5A, no distinct fluorescence emission signal could be observed on the supernatant which was obtained in the absence of phosphate; in contrast, the supernatant obtained

in the presence of phosphate would emit bright red fluorescence signal under UV light irradiation, which was consistent with the phenomena shown in the Inset of Figure 2A. By plotting fluorescence emission enhancement (F/F_0) against the phosphate concentration, where F_0 and F were the fluorescence emission intensities before and after exposure to the analyte, respectively, a good linear correlation could be obtained over a wide concentration range from 0.25 to 100 μM, as depicted in Figure 5B. More than 200-fold fluorescence enhancement of the PCN-222 NR-based nanoprobe was observed after the exposure to phosphate with the concentration of 100 μM. The magnitude of fluorescence enhancement in this work was much higher than those in the previous nanomaterial-based fluorescence "Signal-On" sensors for phosphate.[23,33,34,38] In addition, the limit of detection in the fluorescent detection mode was estimated to be as low as 0.023 μM, which was much lower than the maximum concentration allowed in the environmental or drinking water[39,40] and demonstrated the high sensitivity of the fluorescent detection mode towards phosphate. As is well-known, the buffer pH may affect the analytical performance of the proposed nanoprobe. The buffer pH dependence of the fluorescence emission enhancement was explored, as depicted in Figure 5C. The fluorescence emission enhancement increased with the buffer pH in the range of 5.5-6.5, and then dropped at high pH value (6.5-8.0). Thus, the optimal buffer pH in the fluorescent detection mode was set at 6.5. For a newly proposed sensing strategy, besides sensitivity, the selectivity should also be of great importance for its practical application. The potential interfering species, including Cl^-, SO_4^{2-}, NO_3^-, NO_2^-, Ac^-, CO_3^{2-}, GSH, Ca^{2+}, K^+, Na^+, and Mg^{2+}, were tested under the same condition for their possible effects on the fluorescence emission signal of the proposed nanoprobe. As depicted in Figure 5D, negligible change on the fluorescence emission signal was observed after the exposure to the potential interfering species with the same concentration of 100 μM, whereas the exposure to phosphate could greatly enhance the fluorescence emission signal, confirming the excellent selectivity of the PCN-222 NR-based fluorescent nanoprobe towards phosphate over other interfering species.

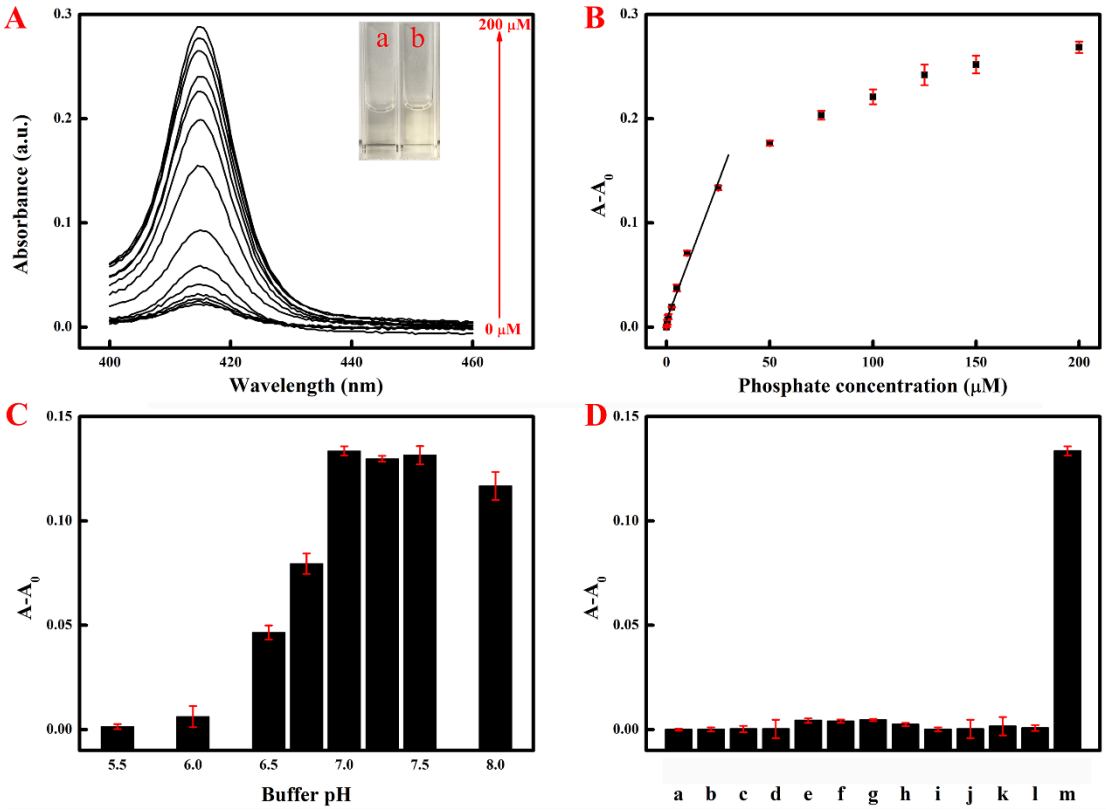

Figure 6. Colorimetric detection mode for phosphate. (A) UV-vis absorbance spectra of supernatant obtained by incubating PCN-222 NRs with phosphate at different concentrations (0-200 μM) in the HEPES buffer solution (20 mM, pH 7.0), (B) Plot of UV-vis absorbance enhancement (A-A_0) against phosphate concentration, (C) The effect of buffer pH on the UV-vis absorbance enhancement, (D) Selectivity experiments, a) blank, b) Cl^-, c) SO_4^{2-}, d) NO_3^-, e) NO_2^-, f) Ac^-, g) CO_3^{2-}, h) GSH, i) Ca^{2+}, j) K^+, k) Na^+, l) Mg^{2+}, m) phosphate with the concentration of 25 μM, where A_0 and A represented UV-vis absorbance intensities of the nanoprobe before and after exposure to the respective analyte, respectively. Inset in Figure 6A: photographs of supernatant obtained in the (a) absence and (b) presence of phosphate under ambient light.

Furthermore, for the colorimetric detection mode, the effect of phosphate concentration on the UV-vis absorbance signal was also investigated. Figure 6A displayed the UV-vis absorbance spectra of the supernatant obtained by incubating PCN-222 NRs with phosphate at different concentrations and subsequently centrifuging. Similar to the fluorescent detection mode (Figure 5), the UV-vis absorbance intensity increased proportionally with the phosphate concentration in the range from 0 μM to 200 μM. The inset of Figure 5A displayed the photographs of the supernatant obtained in the absence and presence of phosphate under ambient light, respectively. A light-yellow color could be observed on the supernatant obtained in the presence of phosphate, whereas the supernatant obtained in the absence of phosphate was transparent. In addition, the UV-vis absorbance enhancement (A-A_0) linearly correlated with the

phosphate concentration from 0.25-25 μM, as depicted in Figure 6B, where A_0 and A were the UV-vis absorbance intensities of the PCN-222 NR-based nanoprobe before and after exposure to the analyte. The limit of detection in the colorimetric detection mode was estimated to be 0.22 μM, demonstrating the good sensitivity of the proposed colorimetric detection mode proposed in this work. The buffer pH on the UV-vis absorbance enhancement was also optimized, as depicted in Figure 6C. The UV-vis absorbance enhancement increased with buffer pH in the range of 5.5-7.0 and dropped slightly at higher pH (7.0-8.0). As such, the colorimetric detection mode was performed in the buffer solution at the optimal pH of 7.0. In addition, the selectivity of the colorimetric sensing strategy proposed in this work was investigated. Figure 6D displayed the UV-vis absorbance change of the PCN-222 NR-based nanoprobe in the presence of potential interfering species as well as phosphate. It was observed that except phosphate, other potential interfering species (i.e., Cl^-, SO_4^{2-}, NO_3^-, NO_2^-, Ac^-, CO_3^{2-}, GSH, Ca^{2+}, K^+, Na^+, and Mg^{2+}) with the same concentration of 25 μM did not induce significant change on the UV-vis absorbance signals, indicating the excellent selectivity of the proposed colorimetric nanoprobe towards phosphate. It should be noted that the enhancement on the fluorescence emission and UV-vis absorbance signals was presented in different forms (i.e., F/F_0 vs. A-A_0) due to the inherent difference on the resolution as well as instrument of fluorescence and UV-vis absorbance techniques. Additionally, different optimal buffer pH was employed in the fluorescent and colorimetric detection modes. The limit of detection in the colorimetric detection mode was higher than that in the fluorescent detection mode, which could be attributed to the inherit sensitivity of fluorescence technique. The similar phenomena have been reported in the previous dual-modal sensing strategies.[24,41]

Table 1. Comparison of analytical performance of different probes for phosphate.

Probe	Sensing Type	Linear Range (μM)	Detection Limit (μM)	Ref.
AgNC	Ratiometric fluorescence	1-100	0.06	32
Tb-MOF	Fluorescence signal-off	40-400	35	42
Eu-BTB MOF	Fluorescence signal-off	0-1000	10	43
Europium-adjusted carbon dot	Fluorescence signal-on	0.4-15	0.051	23
Rhodamine 6G naphthylurea conjugate	Fluorescence signal-on	1-10	0.015	26
Ru^{II} complex	Fluorescence signal-on	0-5.0	0.28	27
Coumarin fluorophore-based compound	Fluorescence signal-on	0-200	0.811	28
UiO-66-NH_2 MOF	Fluorescence signal-on	5-150	1.25	33
UiO-TCPP MOF	Fluorescence signal-on	0.5-105	unavailable	34
ZnO QDs-MOF	Fluorescence signal-on	0.5-12	0.053	38
PCN-222 NR	Fluorescence signal-on	0.25-100	0.023	This work
PCN-222 NR	Absorbance signal-on	0.25-25	0.22	This work

Table 2. Determination of phosphate in real sample.

		Fluorescent Detection Mode			**Colorimetric Detection Mode**[a]		
Sample	Spiked (μM)	Found (μM)	Recovery (%)	RSD (%)	Found (μM)	Recovery (%)	RSD (%)
Drinking Water	0	Not detected	-	-	Not detected	-	-
	25	25.4	101.6	2.86	24.8	99.2	3.38
	75	78.8	105.1	0.44	74.5	99.3	1.13
Tap Water	0	Not detected	-	-	Not detected	-	-
	25	25.2	100.8	4.04	25.8	103.2	3.38
	75	73.7	98.3	0.57	73.5	98.0	1.95

[a]The samples were 10-fold diluted before measurements.

Taken together, PCN-222 NRs could be employed as a high-efficiency nanoprobe for the sensitive and selective determination of phosphate over a wide concentration range with a low detection limit. The analytical performance of the presently proposed nanoprobe was comparable or somewhat better than the previous reported fluorescent/colorimetric sensors developed for phosphate detection, as listed in Table 1. In order to further evaluate the potential application of the proposed dual-modal nanoprobe in the routine analysis, the PCN-222 NR-based nanoprobe was applied for the determination of phosphate in different water sources (i.e., tap water, drinking water). As listed in Table 2, the analytical results obtained by this dual-modal nanoprobe proposed in this work were satisfactory with good accuracy and

precision, validating the practicality of the PCN-222 NR-based nanoprobe for phosphate detection in the water monitoring. To the best of our knowledge, it is the first report on the dual-modal “Signal-On” PCN-222 NR-based nanoprobe towards phosphate.

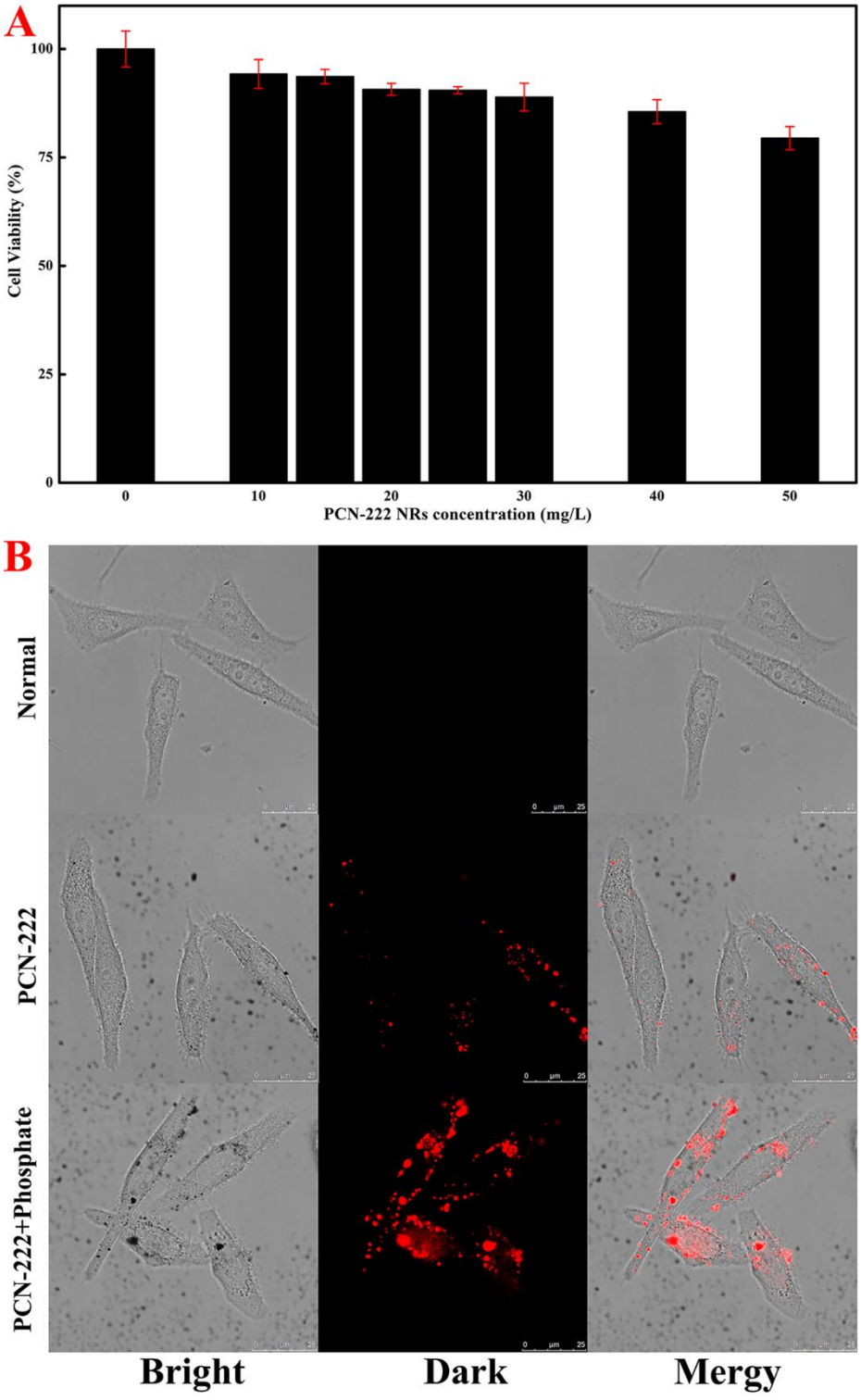

Figure 7. (A) Cell viability of HeLa cells after incubation with PCN-222 NRs at various concentrations for 24 h, (B) Confocal images of HeLa cells under different conditions: normal HeLa cells, HeLa cells cultured with PCN-222 NRs, and HeLa cells cultured with PCN-222 NRs and followed by incubation with phosphate.

Recently, phosphate in the biological medium has also been paid more and more attention due to the unique and important behaviors of phosphate in the biological process. Encouraged by the "Signal-On" effect of phosphate on the fluorescence emission signal of the PCN-222 NR-based nanoprobe, as presented in the above in-vitro experiments, we anticipated that PCN-222 NRs could also employed as the probe for the intracellular imaging of phosphate. Firstly, the standard MTT assay was conducted in HeLa cells to evaluate the potential cytotoxicity and biocompatibility of PCN-222 NRs. As depicted in Figure 7A, after incubating with various concentrations of PCN-222 NRs up to 24 h, the cell viability was ca. 80 % for HeLa cells even the PCN-222 NRs concentration was as high as 50 mg L^{-1}, and the low-toxic nature of PCN-222 NRs against HeLa cells was confirmed. The similar results were reported in the previous work based on zirconium MOFs,[19,20,44] revealing their acceptable biocompatibility, low cytotoxicity as well as great potential in bioapplications. Then, in order to investigate the capability of the proposed PCN-222 NR-based nanoprobe for intracellular phosphate imaging, we incubated HeLa cells with PCN-222 NRs in the absence and presence of phosphate, respectively, as shown in Figure 7B. No fluorescence signal was detected on control group (normal cells), which were not incubated with PCN-222 NRs. After incubation with PCN-222 NRs, only faint red fluorescence signal appeared, which may be attributed to the weak fluorescence emission of PCN-222 NRs. It also verified the successful uptake of PCN-222 NRs into HeLa cells. In contrast, when cells were incubated with exogenous phosphate in the presence of PCN-222 NRs, much stronger red fluorescence emission could be readily observed. The similar "Signal-On" phenomena were reported on previous fluorescent probes for intracellular phosphate imaging.[26,28] Furthermore, the distinct red fluorescence signal observed on HeLa cells in the presence of phosphate was good agreement with the results observed in the in-vitro experiments, validating the availability of PCN-222 NRs as fluorescence probe for bioimaging as well as other fundamental biological research.

Conclusions

In summary, for the first time, we successfully developed a novel PCN-222 NR-based dual-modal (fluorescent and colorimetric) “Signal-On” nanoprobe for sensitive and selective determination of phosphate. The nanostructured porphyrinic MOFs, PCN-222 NRs were prepared under solvothermal reaction by using zirconium and TCPP as the metal node and organic ligand, respectively. On the basis of the significantly high coordination interaction and specificity between zirconium node in the framework of PCN-222 NRs and phosphate, the structure collapse of PCN-222 NRs could be selectively triggered by phosphate, followed by the release of the free TCPP from the framework of PCN-222 NRs, which would result in the great enhancement on the fluorescence emission and UV-vis absorbance signals. The practical application of the PCN-222 NR-based nanoprobe for phosphate determination in real water samples was demonstrated. Furthermore, this nanoprobe with low cytotoxicity and good compatibility was successfully employed for the intracellular imaging of phosphate. These findings would open a promising avenue to design diverse NMOFs for broadening their potential applications in the sensing and biological fields.

Acknowledgement

This work was supported by National Natural Science Foundation of China (Nos. 21405144, 31771077 and 81471747), Hong Kong Polytechnic University Postdoctoral Fellowship Scheme (1-YW1L), Guang Dong-Hong Kong Technology Cooperation Funding Scheme (2016A050503027) and the internal fund of the Hong Kong Polytechnic University (No. 1-ZVJ7 and 4-BCCC).

Reference

1. Peng, Y.; Li, Y. S.; Ban, Y.; Jin, H.; Jiao, W.; Liu, X.; Yang, W., Metal-organic framework nanosheets as building blocks for molecular sieving membranes. *Science* **2014,** *346* (6215), 1356-1359.

2. Rodenas, T.; Luz, I.; Prieto, G.; Seoane, B.; Miro, H.; Corma, A.; Kapteijn, F.; Llabrés i Xamena, F. X.; Gascon, J., Metal-organic framework nanosheets in polymer composite materials for gas separation. *Nat. Mater.* **2015,** *14* (1), 48-55.

3. Gu, Z.; Park, J.; Raiff, A.; Wei, Z.; Zhou, H., Metal-organic frameworks as biomimetic catalysts. *ChemCatChem* **2014,** *6* (1), 67-75.

4. Jiao, L.; Wang, Y.; Jiang, H.; Xu, Q., Metal-Organic Frameworks as Platforms for Catalytic Applications. *Adv. Mater.* **2017,** *30* (37), 1703663.

5. Cai, W.; Chu, C.; Liu, G.; Wáng, Y., Metal-Organic Framework-Based Nanomedicine Platforms for Drug Delivery and Molecular Imaging. *Small* **2015,** *11* (37), 4806-4822.

6. Wu, M.; Yang, Y., Metal-Organic Framework (MOF)-Based Drug/Cargo Delivery and Cancer Therapy. *Adv. Mater.* **2017,** *29* (23), 1606134.

7. Lu, K.; Aung, T.; Guo, N.; Weichselbaum, R.; Lin, W., Nanoscale Metal-Organic Frameworks for Therapeutic, Imaging, and Sensing Applications. *Adv. Mater.* **2018,** *30* (37), 1707634.

8. Kreno, L.; Leong, K.; Farha, O.; Allendorf, M.; Van Duyne, R.; Hupp, J., Metal-organic framework materials as chemical sensors. *Chem. Rev.* **2011,** *112* (2), 1105-1125.

9. Deng, J.; Wang, K.; Wang, M.; Yu, P.; Mao, L., Mitochondria Targeted Nanoscale Zeolitic Imidazole Framework-90 for ATP Imaging in Live Cells. *J. Am. Chem. Soc.* **2017,** *139* (16), 5877-5882.

10. Huang, Y.; Zhao, M.; Han, S.; Lai, Z.; Yang, J.; Tan, C.; Ma, Q.; Lu, Q.; Chen, J.; Zhang, X.; Zhang, Z.; Li, B.; Chen, B.; Zong, Y.; Zhang, H., Growth of Au Nanoparticles on 2D Metalloporphyrinic Metal-

Organic Framework Nanosheets Used as Biomimetic Catalysts for Cascade Reactions. *Adv. Mater.* **2017,** *29* (32), 1700102.

11. Ling, P.; Lei, J.; Ju, H., Nanoscaled Porphyrinic Metal-Organic Frameworks for Electrochemical Detection of Telomerase Activity via Telomerase Triggered Conformation Switch. *Anal. Chem.* **2016,** *88* (21), 10680-10686.

12. Yang, X.; Yu, Y.; Peng, L.; Lei, Y.; Chai, Y.; Yuan, R.; Zhuo, Y., Strong Electrochemiluminescence from MOF Accelerator Enriched Quantum Dots for Enhanced Sensing of Trace cTnI. *Anal. Chem.* **2018,** *90* (6), 3995-4002.

13. Zhang, G.; Zhuang, Y.; Shan, D.; Su, G.; Cosnier, S.; Zhang, X., Zirconium-Based Porphyrinic Metal-Organic Framework (PCN-222): Enhanced Photoelectrochemical Response and Its Application for Label-Free Phosphoprotein Detection. *Anal. Chem.* **2016,** *88* (22), 11207-11212.

14. Wang, J.; Fan, Y.; Lee, H.; Yi, C.; Cheng, C.; Zhao, X.; Yang, M., Ultrasmall Metal-Organic Framework Zn-MOF-74 Nanodots: Size-Controlled Synthesis and Application for Highly Selective Colorimetric Sensing of Iron(III) in Aqueous Solution. *ACS Applied Nano Materials* **2018,** *1* (7), 3747-3753.

15. Li, L.; Shen, S.; Lin, R.; Bai, Y.; Liu, H., Rapid and specific luminescence sensing of Cu(ii) ions with a porphyrinic metal-organic framework. *Chem. Commun.* **2017,** *53* (72), 9986-9989.

16. Liu, W.; Wang, Y.; Li, Y.; Cai, S.; Yin, X.; He, X.; Zhang, Y., Fluorescent Imaging-Guided Chemotherapy-and-Photodynamic Dual Therapy with Nanoscale Porphyrin Metal-Organic Framework. *Small* **2017,** *13* (17), 1603459.

17. Park, J.; Jiang, Q.; Feng, D.; Mao, L.; Zhou, H., Size-Controlled Synthesis of Porphyrinic Metal-Organic Framework and Functionalization for Targeted Photodynamic Therapy. *J. Am. Chem. Soc.* **2016,** *138* (10), 3518-3525.

18. Zeng, J.; Zhang, M.; Peng, M.; Gong, D.; Zhang, X., Porphyrinic Metal-Organic Frameworks Coated Gold Nanorods as a Versatile Nanoplatform for Combined Photodynamic/Photothermal/Chemotherapy of Tumor. *Adv. Funct. Mater.* **2018,** *28* (8), 1705451.

19. Zhang, Y.; Wang, F.; Liu, C.; Wang, Z.; Kang, L.; Huang, Y.; Dong, K.; Ren, J.; Qu, X., Nanozyme Decorated Metal-Organic Frameworks for Enhanced Photodynamic Therapy. *ACS Nano* **2018,** *12* (1), 651-661.

20. Chen, H.; Wang, J.; Shan, D.; Chen, J.; Zhang, S.; Lu, X., Dual-Emitting Fluorescent Metal-Organic Framework Nanocomposites as a Broad-Range pH Sensor for Fluorescence Imaging. *Anal. Chem.* **2018,** *90* (11), 7056-7063.

21. Liu, Y.; Moon, S.; Hupp, J.; Farha, O., Dual-Function Metal-Organic Framework as a Versatile Catalyst for Detoxifying Chemical Warfare Agent Simulants. *ACS Nano* **2015,** *9* (12), 12358-12364.

22. Wang, S.; McGuirk, C. M.; Ross, M.; Wang, S.; Chen, P.; Xing, H.; Liu, Y.; Mirkin, C., General and Direct Method for Preparing Oligonucleotide-Functionalized Metal-Organic Framework Nanoparticles. *J. Am. Chem. Soc.* **2017,** *139* (29), 9827-9830.

23. Zhao, H.; Liu, L.; Liu, Z.; Wang, Y.; Zhaoa, X.; Huang, C., Highly selective detection of phosphate in very complicated matrixes with an off-on fluorescent probe of europium-adjusted carbon dots. *Chem. Commun.* **2011,** *47* (9), 2604-2606.

24. Chen, C.; Zhao, J.; Lu, Y.; Sun, J.; Yang, X., Fluorescence Immunoassay Based on the Phosphate-Triggered Fluorescence Turn-on Detection of Alkaline Phosphatase. *Anal. Chem.* **2018,** *90* (5), 3505-3511.

25. Li, J.; Si, L.; Bao, J.; Wang, Z.; Dai, Z., Fluorescence Regulation of Poly(thymine)-Templated Copper Nanoparticles via an Enzyme-Triggered Reaction toward Sensitive and Selective Detection of Alkaline Phosphatase. *Anal. Chem.* **2017,** *89* (6), 3681-3686.

26. Wang, K.; Zhang, S.; Lv, C.; Shang, H.; Jin, Z.; Chen, S.; Zhang, Q.; Zhang, Y.; Hu, Z., A highly sensitive and selective turn-on fluorescent sensor for dihydrogen phosphate in living cells. *Sensors and Actuators B: Chemical* **2017,** *247*, 791-796.

27. Chowdhury, B.; Sinha, S.; Ghosh, P., Selective Sensing of Phosphates by a New Bis-heteroleptic RuII Complex through Halogen Bonding: A Superior Sensor over Its Hydrogen-Bonding Analogue. *Chem. Eur. J.* **2016,** *22* (50), 18051-18059.

28. Guo, L.; Zhang, J.; Liu, X.; Zhang, L.; Zhang, H.; Chen, J.; Xie, X.; Zhou, Y.; Luo, K.; Yoon, J., Phosphate Ion Targeted Colorimetric and Fluorescent Probe and Its Use to Monitor Endogeneous Phosphate Ion in a Hemichannel-Closed Cell. *Anal. Chem.* **2015,** *87* (2), 1196-1201.

29. Shi, B.; Zhang, Y.; Wei, T.; Lin, Q.; Yao, H.; Zhang, P.; You, X., A fluorescent and colorimetric chemosensor for dihydrogen phosphate ions based on 2-pyridine-1H-imidazo [4, 5-b] phenazine–zinc ensemble. *Sensors and Actuators B: Chemical* **2014,** *190*, 555-561.

30. Dwivedi, S.; Gupta, R.; Srivastava, P.; Singh, P.; Koch, B.; Maiti, B.; Misra, A., Dual Fluorophore Containing Efficient Photoinduced Electron Transfer Based Molecular Probe for Selective Detection of Cr^{3+} and PO_4^{3-} Ions through Fluorescence "Turn-On-Off" Response in Partial Aqueous and Biological Medium: Live Cell Imaging and Logic Application. *Anal. Chem.* **2018,** *90* (18), 10974-10981.

31. Chu, T.; Zhang, F.; Wang, Y.; Yang, Y.; Ng, S., A Novel Electrophoretic Deposited Coordination Supramolecular Network Film for Detecting Phosphate and Biophosphate. *Chem. Eur. J.* **2017,** *23* (32), 7748-7754.

32. Dai, C.; Yang, C.; Yan, X., Ratiometric Fluorescent Detection of Phosphate in Aqueous Solution Based on Near Infrared Fluorescent Silver Nanoclusters/Metal-Organic Shell Composite. *Anal. Chem.* **2015,** *87* (22), 11455-11459.

33. Yang, J.; Dai, Y.; Zhu, X.; Wang, Z.; Li, Y.; Zhuang, Q.; Shi, J.; Gu, J., Metal-organic frameworks with inherent recognition sites for selective phosphate sensing through their coordination-induced fluorescence enhancement effect. *J. Mater. Chem. A* **2015,** *3* (14), 7445-7452.

34. Zhang, W.; Xu, J.; Li, P.; Gao, X.; Zhang, W.; Wang, H.; Tang, B., Treatment of hyperphosphatemia based on specific interactions between phosphorus and Zr(iv) active centers of nano-MOFs. *Chemical Science* **2018,** *9* (38), 7483-7487.

35. Giménez-Marqués, M.; Bellido, E.; Berthelot, T.; Simón-Yarza, T.; Hidalgo, T.; Simón-Vázquez, R.; González-Fernández, Á.; Avila, J.; Asensio, M.; Gref, R.; Couvreur, P.; Serre, C.; Horcajada, P., GraftFast Surface Engineering to Improve MOF Nanoparticles Furtiveness. *Small* **2018,** *14* (40), 1801900.

36. Chen, Y.; Li, P.; Modica, J.; Drout, R.; Farha, O., Acid-Resistant Mesoporous Metal-Organic Framework toward Oral Insulin Delivery: Protein Encapsulation, Protection, and Release. *J. Am. Chem. Soc.* **2018,** *140* (17), 5678-5681.

37. Gibson, L.; Wright, D., Sensitive Method for Biomolecule Detection Utilizing Signal Amplification with Porphyrin Nanoparticles. *Anal. Chem.* **2016,** *88* (11), 5928-5933.

38. Zhao, D.; Wan, X.; Song, H.; Hao, L.; Su, Y.; Lv, Y., Metal-organic frameworks (MOFs) combined with ZnO quantum dots as a fluorescent sensing platform for phosphate. *Sensors and Actuators B: Chemical* **2014,** *197,* 50-57.

39. Cheng, W.; Sue, J.; Chen, W.; Chang, J.; Zen, J., Activated Nickel Platform for Electrochemical Sensing of Phosphate. *Anal. Chem.* **2010,** *82* (3), 1157-1161.

40. Song, X.; Ma, Y.; Ge, X.; Zhou, H.; Wang, G.; Zhang, H.; Tang, X.; Zhang, Y., Europium-based infinite coordination polymer nanospheres as an effective fluorescence probe for phosphate sensing. *RSC Adv* **2017,** *7* (14), 8661-8669.

41. Yun, W.; Wu, H.; Liu, X.; Zhong, H.; Fu, M.; Yang, L.; Huang, Y., Ultra-sensitive fluorescent and colorimetric detection of UO_2^{2+} based on dual enzyme-free amplification strategies. *Sensors and Actuators B: Chemical* **2018,** *255,* 1920-1926.

42. Asha, K. S.; Bhattacharjee, R.; Mandal, S., Complete Transmetalation in a Metal-Organic Framework by Metal Ion Metathesis in a Single Crystal for Selective Sensing of Phosphate Ions in Aqueous Media. *Angew. Chem. Int. Ed.* **2016,** *55* (38), 11528-11532.

43. Xu, H.; Cao, C.; Zhao, B., A water-stable lanthanide-organic framework as a recyclable luminescent probe for detecting pollutant phosphorus anions. *Chem. Commun.* **2015,** *51* (51), 10280-10283.

44. Zeng, J.; Zou, M.; Zhang, M.; Wang, X.; Zeng, X.; Cong, H.; Zhang, X., π-Extended Benzoporphyrin-Based Metal-Organic Framework for Inhibition of Tumor Metastasis. *ACS Nano* **2018,** *12* (5), 4630-4640.